Surface & Coatings Technology 363 (2019) 210–220

Contents lists available at ScienceDirect

Surface & Coatings Technology

journal homepage: www.elsevier.com/locate/surfcoat

Microstructural evolution of alumina coatings by a novel long laminar plasma spraying method

Sen-Hui Liu[a], Hui-Yu Zhang[a], Yue-Peng Wang[a], Gang Ji[a], Lu Li[b], Pan Xu[b], Jia-Hua Huang[b], Shan-Lin Zhang[a], Cheng-Xin Li[a,*], Chang-Jiu Li[a]

[a] State Key Laboratory for Mechanical Behavior of Materials, School of Materials Science and Engineering, Xi'an Jiaotong University, Xi'an, Shaanxi 710049, China
[b] Zhenhuo Plasma Technology. Inc, Chendu, Sichuan 610065, China

ARTICLE INFO

Keywords:
Laminar plasma jet
Thermal spraying
Alumina coatings
Particles velocity
Thermal conductivity

ABSTRACT

A super long and stable laminar plasma jet was used in the atmospheric plasma spray process in this work. Microstructures evolution and properties of alumina coatings that were obtained using a long spraying distance ranging from 200 mm to 350 mm in an atmospheric environment were studied in this work. These processes were carried out by using a total gas flow rate of 14 slpm with 70% nitrogen and 30% argon in volume and output power of 25.4 kW (current of 160 A). A long particle residence time was obtained in this study, which compared with other current atmospheric plasma spray methods. The microstructures of coatings showed the multi-island protrusions on the top surfaces and overlapped lamellar splats at the fracture surfaces. The microstructural evolution was significantly affected by the heating and motion behaviors of alumina particles when these were flowing in the long laminar plasma jet at different spraying distances.

1. Introduction

The widely used atmospheric plasma spraying systems commonly contain the plasma generation unit, the powder materials supply unit and other auxiliary units (robot, dust extraction device, etc.). The plasma generation unit includes the plasma torch, power supply device and water-cooling device. The plasma torch that often uses a type of direct current non-transferred arc plasma torch is one of the crucial parts in the thermal spraying technology.

For example, the commercial Sulzer Metco F4 torch and Praxair SG-100 Torch are two of the most flexible and durable plasma spraying torches in industry applications. Duan and Heberlein, Nogues et al. and Rat et al. found that the current and voltage characteristic of output power were all at the high working current ($\geq$ 300 A) and low working voltage ($\geq$ 30 V) [1–3], especially for the working voltage with a highly fluctuation frequency, which are two of the main factors to induce the instability and turbulence inside the plasma torch and downstream plasma jet. The output power and total gas flow rate usually exceed 30 kW and 40 slpm, respectively. This processes also produce a huge noise at the same time due to the strongly air entrainment (usually 120–130 dB). As the length of pure argon plasma jet was < 200 mm in the atmospheric environment and the overall jet only existed less than one-third argon [4].

Therefore, the velocity and temperature gradients of these plasma jets from conventional direct current non-transferred arc plasma torches are significantly high in the atmospheric environment. The spraying distances were usually in the range from 80 mm to 200 mm in the atmospheric environment. Planche et al., Li et al. and Zhao et al. investigated that the melting state of particles was significantly influenced by the particles velocity [5–7]. In the experiment, the maximum temperature and velocity of the plasma jet were all increased simultaneously with the increasing of output power of the plasma torch. However, the length of plasma jet was not increased significantly at the same time. Thus, the particle flight time in the plasma jet that can strongly affect the particle melting behavior was not increased at the same time.

A novel long laminar plasma jet that was used in the atmospheric thermal spray process was presented in this work. This novel spray method can significantly improve the particle heating and accelerating distance during the plasma spray process and obtain different microstructures of coatings. The velocity and surface temperature of alumina particles when these were flowing inside the long laminar plasma jet at

Abbreviations: APS, atmospheric plasma spray; HVOF, high velocity oxy-fuel; SD, spraying distance; SEM, scanning electron microscopy; XRD, X-ray diffraction

* Corresponding author at: School of Materials Science and Engineering, Xi'an Jiaotong University, State Key Laboratory for Mechanical Behavior of Materials, Xi'an, Shaanxi 710049, China.
E-mail address: licx@xjtu.edu.cn (C.-X. Li).

https://doi.org/10.1016/j.surfcoat.2019.02.018
Received 9 September 2018; Received in revised form 7 January 2019; Accepted 6 February 2019
Available online 07 February 2019
0257-8972/

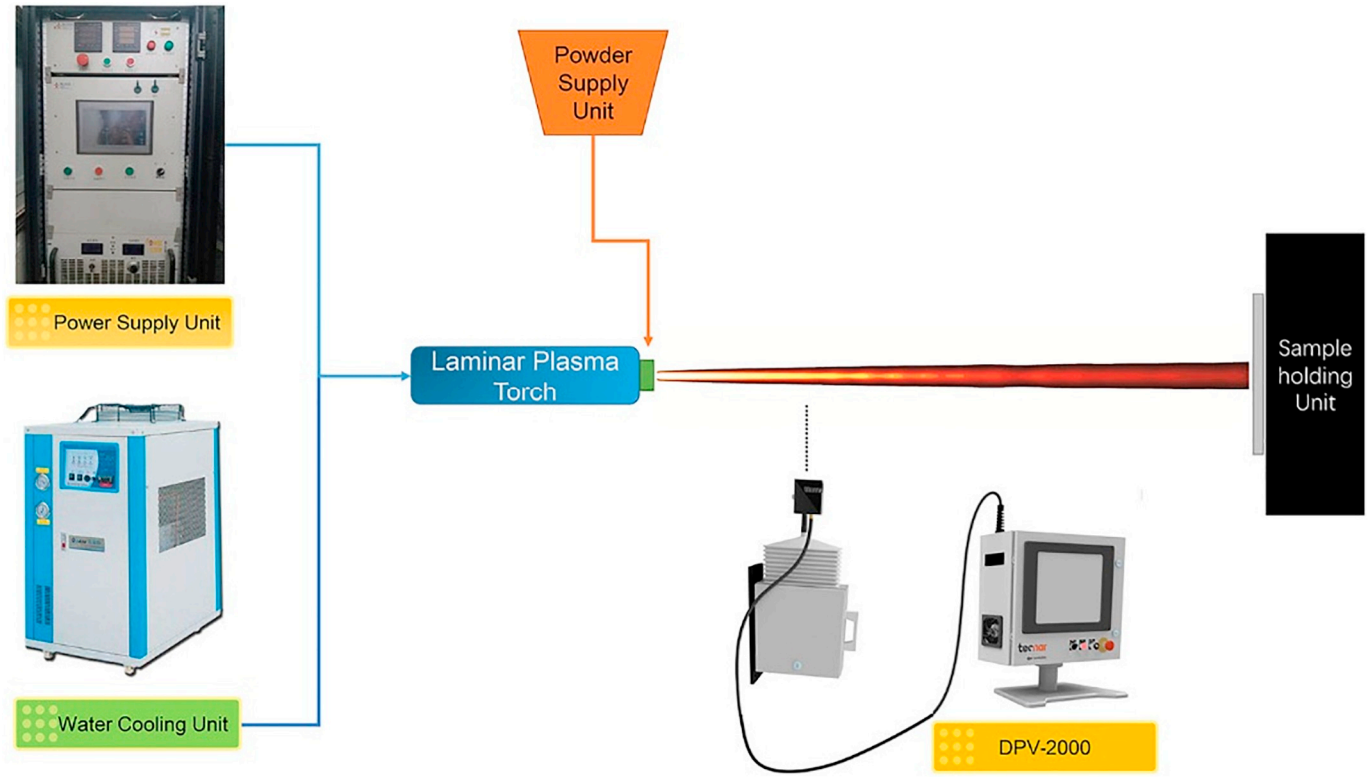

Fig. 1. Schematic diagram of this laminar plasma spraying system and in-situ measurement.

Table 1
Experiment parameters of laminar plasma spray system.

Spraying parameters	Value
Output power/kW	25–26
Spray scan velocity/m/ s	0.6
Spray scan interval/mm	4
Spray distance/mm	200–350
Plasma gas N_2/Ar	7:3 (by volume)
Total flow rate of gas/slpm	14
Feedstock	Al_2O_3 (Metco 6062)
Particle feed rate/g·min^{-1}	8

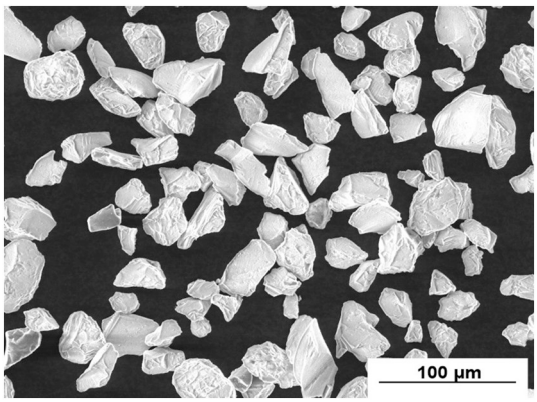

Fig. 2. The morpology of the initial alumina powders.

different spraying distances were measured in-situ on experiment. Microstructures variation of alumina coatings that were deposited at the long spraying distances ranging from 200 mm to 350 mm were discussed in this manuscript. The coatings properties also studied in following. The effects of particles heating state to microstructure characteristics and coating properties were also investigated in this work.

2. Experimental processes

2.1. Atmospheric laminar plasma spray system and feed materials

Fig. 1 showed the schematic diagram of atmospheric laminar plasma spray process. It included power supply unit, water cooling unit, sample holding unit, powder supply unit and the plasma torch [8]. The rated power is 30 kW. The all experiment process was carried out on this system. The working gases chose the mixtures of 70% nitrogen and 30% argon in volume [9]. The details of spraying parameters presented in Table 1.

In this study, a super long spraying distances (200, 250, 300, 350 mm) were using by this novel plasma spraying system. The alumina powders (*Metco 6062*, $-45\sim+22$ μm, *Sulzer Metco*, *Westbury*, *USA*) were used as the initial feed material (Fig. 2), which were injected without carrier gas at the radial direction near the torch nozzle [10]. The prepared substrates were 304 stainless steel that under sand blasting before spraying experiment. The substrates that used in single-scanning deposited splats were polished with abrasive papers.

The DPV-2000 particle diagnostics system (Technar, DVP-2000, Canada) was used to analyze the characteristics of in-flight particles during spray process in several specific positions of the laminar plasma jet (1000 particles per position). The surface temperature (two-wavelength pyrometry) and the velocity of the spray particles (light barrier principle) were all be measured simultaneously [11].

2.2. Characterization of coatings

The microstructure observations of coatings used the scanning electron microscope (SEM VEGA II, TESCAN, Czech), including the top surfaces, cross sections and fracture surfaces. The constituent identification was used by X-ray diffraction (XRD, Rigaku D/max 2400, Japan).

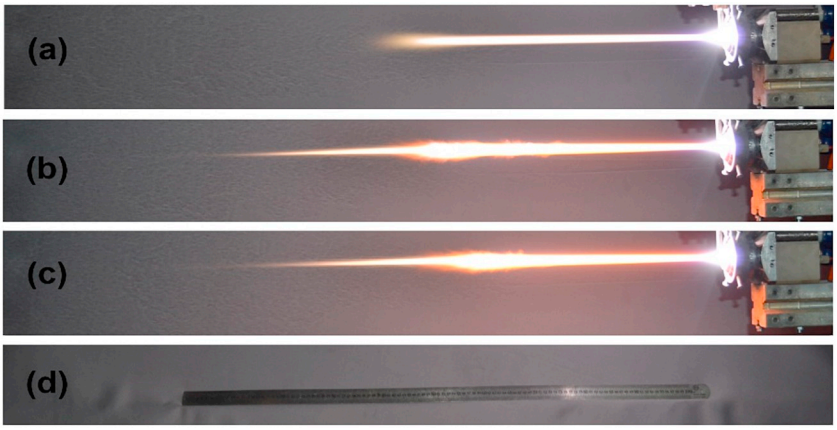

Fig. 3. Photos of the laminar plasma jet (a), particles heating and accelerating over two consecutive seconds, after 1 s of (b), 2 s of (c) and a ruler of 1000 mm at the same position (d).

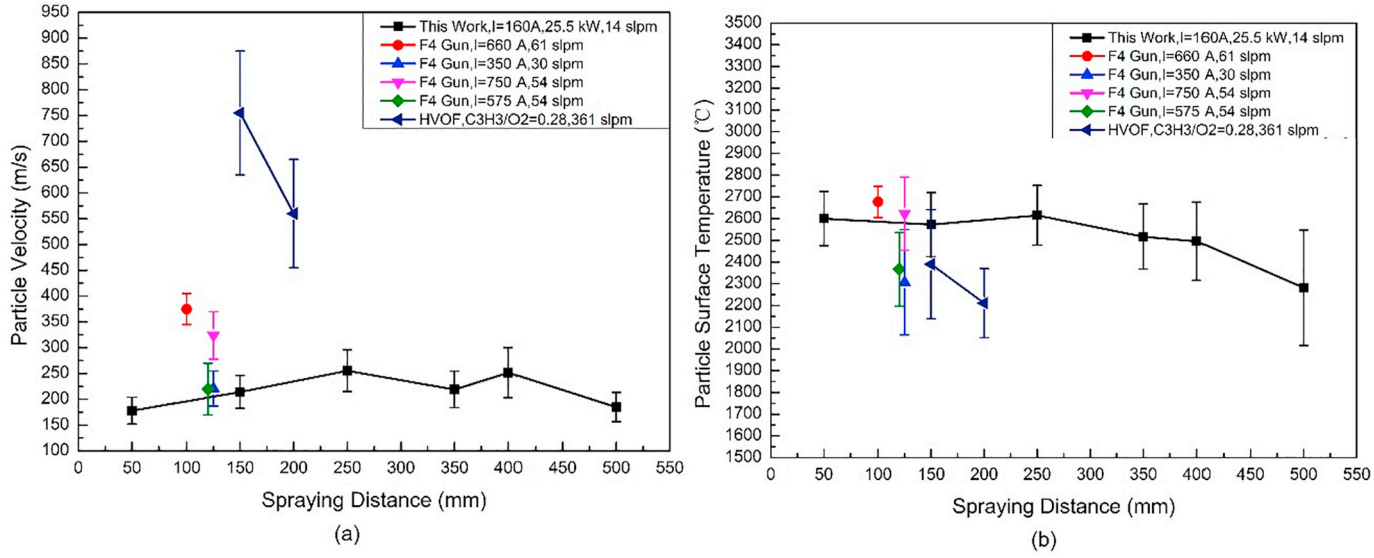

Fig. 4. Particle velocity (a) and particle surface temperature (b) in the laminar plasma jet at different positions from the nozzle exit and comparing with other published results.

The polished cross-section porosity of the coatings was determined by image analyzing method using SEM images. The Micro Vickers Hardness Meter was measured the hardness of the coating on polished cross-section (300 gf, 30 s, BUEHLER MICROMET5104, USA).

The top surface roughness of the coatings was measured by Keyence Color 3D Laser Scanning Microscope (VK-9700, Violet Laser, Japan). It is equipped with laser confocal technology that obtains images with a large depth of field. That are in focus across the entire screen and detect the finest details in the sample shape data. Use of this type of optics as a sensor allows for the maximum possible amount of light to reach the photoreceptor and allows changes in the focal point to be measured and used as height information [12]. The detect area of photos in a sample is about 1 mm × 1.4 mm. The mean roughness and error bars were calculated from five photos (five different positions) in a sample.

The Laser Flash Method (ASTM, E1461) was used to measure the thermal diffusivities of coatings by Netzsch LFA-427 [13]. The differential scanning calorimeters (Netzsch 404, Germany) was used to measure the heat capacity of the coatings. Each sample was measured three times at one selected temperature.

3. Experimental results

3.1. Characteristics of the particle velocity and surface temperature during spray process

Fig. 3a showed the laminar plasma jet in the atmospheric environment (output power = 25–26 kW, I = 160 A, G = 14 *slpm*, N_2: Ar = 7:3 in volume). Fig. 3b and c showed the photos of heating and accelerating of alumina particles when these were flowing in this long laminar plasma jet over two consecutive seconds.

As Fig. 4 demonstrated the particle velocity (Fig. 4a) and surface temperature (Fig. 4b) in the laminar plasma jet at different positions by

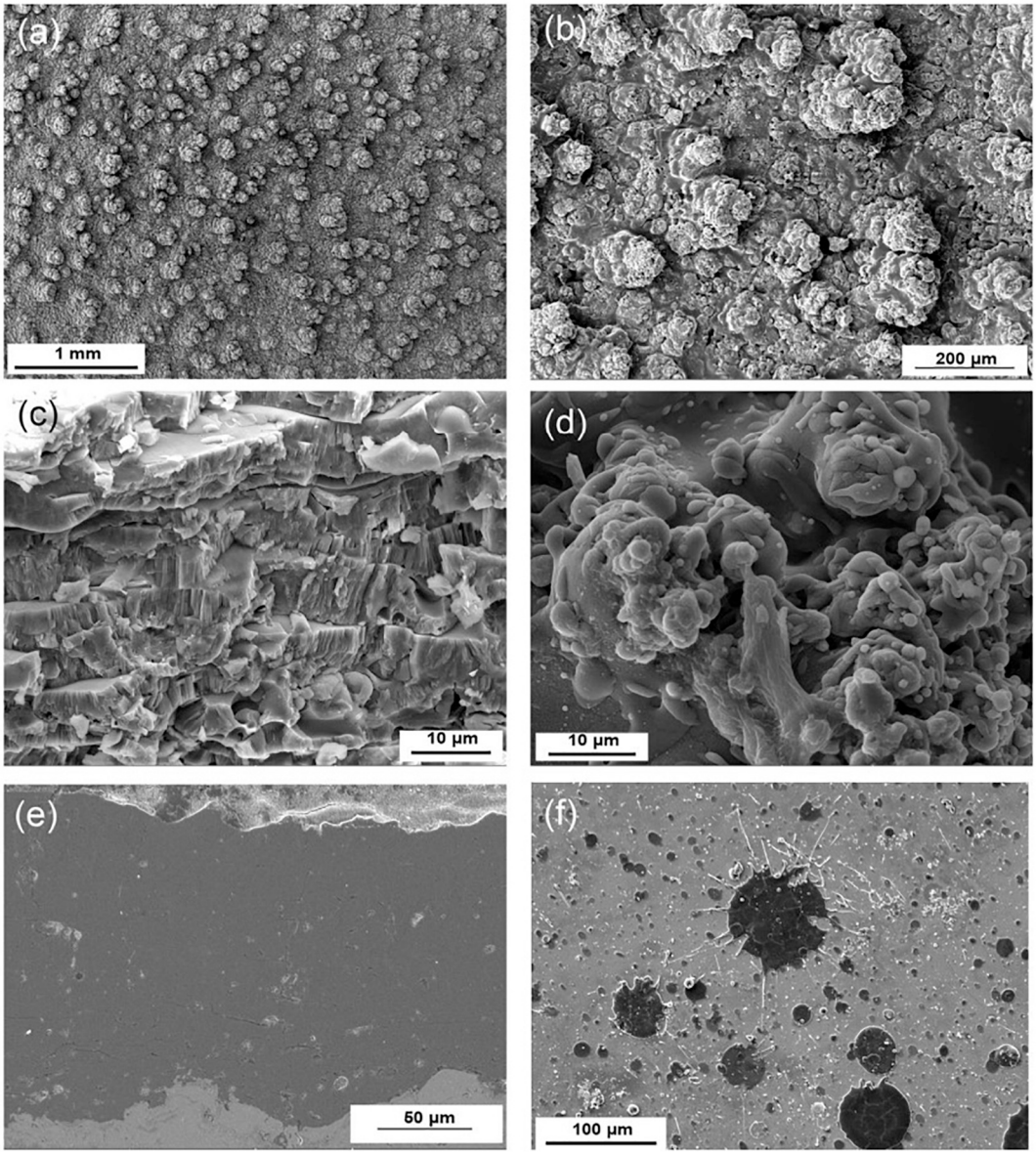

Fig. 5. Top surfaces (a, b, d), fracture surface (c), polished cross-section (e) and single scanning splats (f) of alumina coatings (SD = 200 mm, Sample A).

the DPV-2000 particle diagnostics system (Technar. Inc., Canada). Moreover, the results compared with other three commercial atmospheric plasma spray systems (APS) and one high velocity oxy-fuel spray system (HVOF) as following,

- Planche et al. used APS method (I = 575 A, Ar/H_2 = 40/14 slpm) [5];
- Guessasma et al. used APS method (I = 350 A, 30 slpm and I = 750A, 54 slpm, Al_2O_3-13%TiO_2) [14];
- Yin et al. used APS method (I = 660 A, Ar/H_2 = 49/12 slpm) [15];
- Turunen et al. used HVOF method (C_3H_3/O_2 = 0.28, 361 slpm) [16].

That were all from published papers using alumina powders, except for Guessasma. S. et al. [14] used Al_2O_3-13%TiO_2 powders.

The sensor of DPV-2000 particle diagnostics system had an XY positioning unit which allowed a cross section of the laminar plasma jet to be scanned perpendicularly to the spray axis. In this way, a two-dimensional distribution of the particle characteristics was be determined. The alumina particles were injected at the nozzle exit at the beginning and then be accelerated to 150 m/s–300 m/s at the corresponding distance from the torch nozzle exit ranging from 50 mm to 500 mm. Even it can also detect the particles of mean velocity 185 m/s at the distance of 500 mm from the nozzle exit of the laminar plasma torch. The surface temperature distributions of particles at the distance ranging from 50 mm to 500 mm were all higher than 2000 °C, which increased to the peak value at the distance of 250 mm and then decreased. Comparing with other methods that using much higher input power and gas flow rates, these all possess higher particle velocity at different spraying distances than this work (Fig. 4a), although the distributions of particle surface temperature were not significantly higher than the results of this work (Fig. 4b). Therefore, the alumina particles

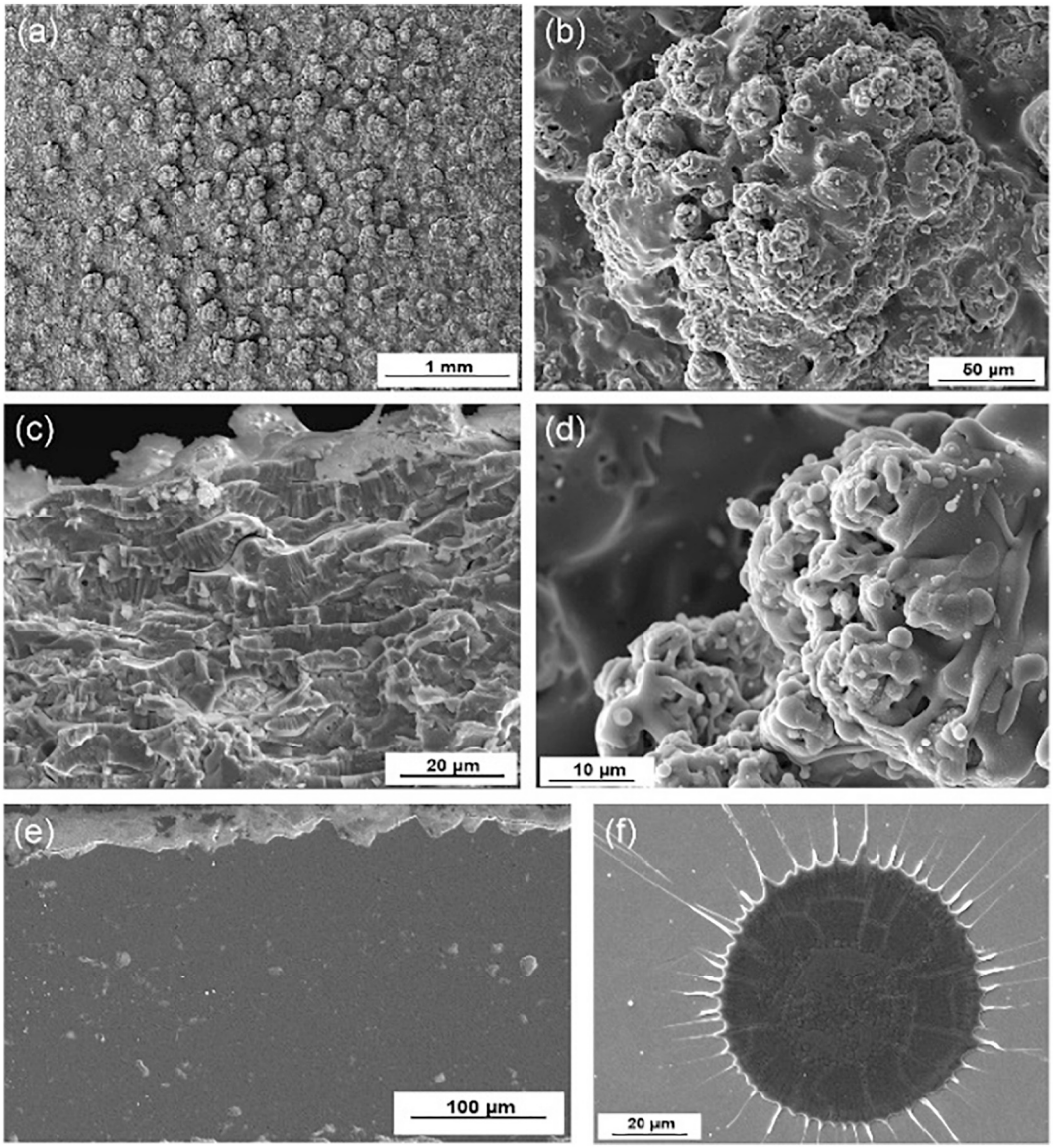

Fig. 6. Top surfaces (a, b, d), fracture surface (c), polished cross-section (e) and single scanning splat (f) of alumina coatings (SD = 250 mm, Sample B).

flowed through a super-long heating and accelerating distance in this work, obtaining a long particle flight time as the relative lower particle velocity and higher particle surface temperature compared with other spraying methods.

3.2. Microscopic observations of alumina coatings

The single scanned splats, top surfaces, fracture surfaces and polished cross-section surfaces of four coatings were shown from Figs. 5 to 8 of sample A to sample D in Table 2. Fig. 5 showed the microstructure observations of Sample A that deposited at a spraying distance of 200 mm. The top surface of coating was characterized by the orderly distributed multi-island protrusions with overlapped splats (Fig. 5a, b, d) that obtained at the torch move velocity of 0.6 m/s and interval of 4 mm during spray process. The top of multi-island protrusions was composed of the aggregation of molten droplets without distinctly unmelted particles from the high magnification SEM observation at Fig. 5d. The fracture section presented a typically lamellar structure that contained layers of flattening particles (Fig. 5c) and the polished cross-section of coating presented voids and pores (Fig. 5e), which were similar to the results from the conventional atmospheric plasma sprayed coatings [6,19,23]. The maximum diameter of splats in Fig. 5f that deposited after single scanning was < 100 μm at the polished surface of substrate (surface temperature of 473 K).

Fig. 6 demonstrated the microstructures of sample B in Table 2. It was deposited at the spraying distance of 250 mm from the nozzle exit of torch and unavailable realized by the conventional atmospheric plasma spraying equipment. There also existed multi-island protrusions structures at the top surface of coatings (Fig. 6a, b) with mean surface roughness of 22 μm (Ra). The solidified micro-droplets aggregated at the top of protrusions and without unmelted particles (Fig. 6c). The polished cross-section and fracture section of coatings all presented typically porous structure and lamellar structure as the results of conventional plasma sprayed alumina coatings. The shape of single splat in

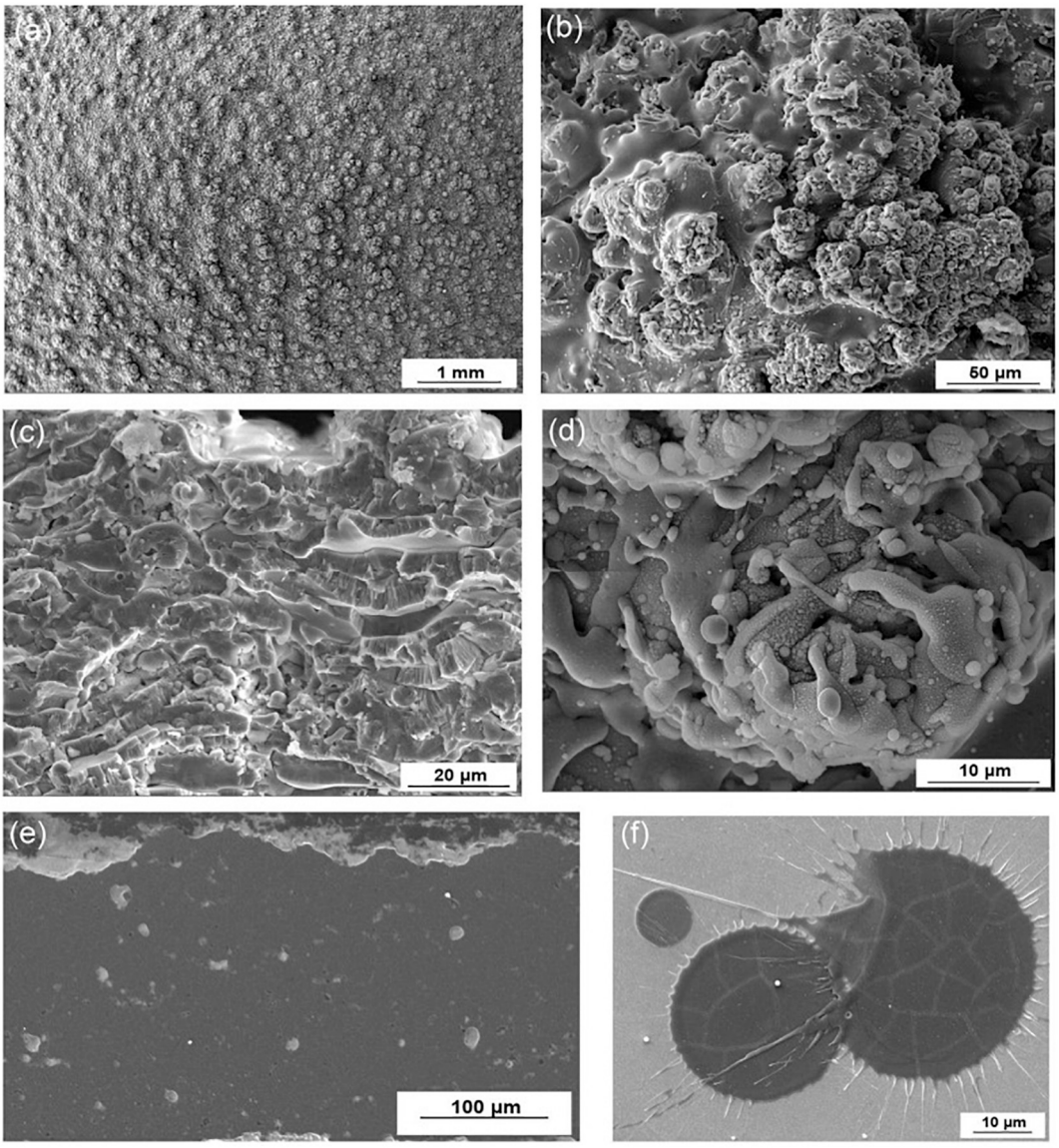

Fig. 7. Top surfaces (a, b, d), fracture surface (c), polished cross-section (e) and single scanning splats (f) alumina coatings (SD = 300 mm, Sample C).

Fig. 6f that was deposited at the substrate temperature of 473 K was similar to a disc-shape with the splashing along its periphery.

The microstructures of coating in Fig. 7 of sample C showed the same results as previous Sample B. These still existed micro - solidified droplets at the tops of multi-island protrusions (Fig. 7a, b, d). The thickness of single lamellar layer was almost < 10 μm from the observation of the fracture surface (Fig. 7c). The shape of single scanned splats also presented mixtures of disc-liked shape with the splashing at the substrate temperature of 473 K.

For the sample that was deposited at the spraying distance of 350 mm, the microstructures of coating were characterized by pores and voids on the cross-section and orderly distributed multi-island protrusions on the top surface (Fig. 8a, b, c, d). The fracture section of coatings showed the typically lamellar structure with overlapped splats (Fig. 8e). The morphology of single-scanning deposited splats almost presented disc-shaped with few splashing and dendritic structures around its periphery (Fig. 8f). The single-scanning splats were deposited on the substrate temperature of 473 K. The diameter of splats on the substrate was < 100 μm.

In experiment, the deposition rate of atmospheric laminar plasma sprayed alumina coatings is about 15%–20% through the calculation from ISO 17386:2017 [17], which is lower than the conventional APS methods. Although the particle feed rate is only 8 g min^{-1}, the particles usage rate is extremely high because of a very focused deposition spot. In some conditions, this process does not need the powders dedusting extraction. For example, at the longest spraying distance of 350 mm, the coating with a thickness of about 200 μm need through 20 repeated scanning of spraying in experiment.

Therefore, according to the above results, the initial alumina powders of polygonal morphology are totally melted into droplets at the

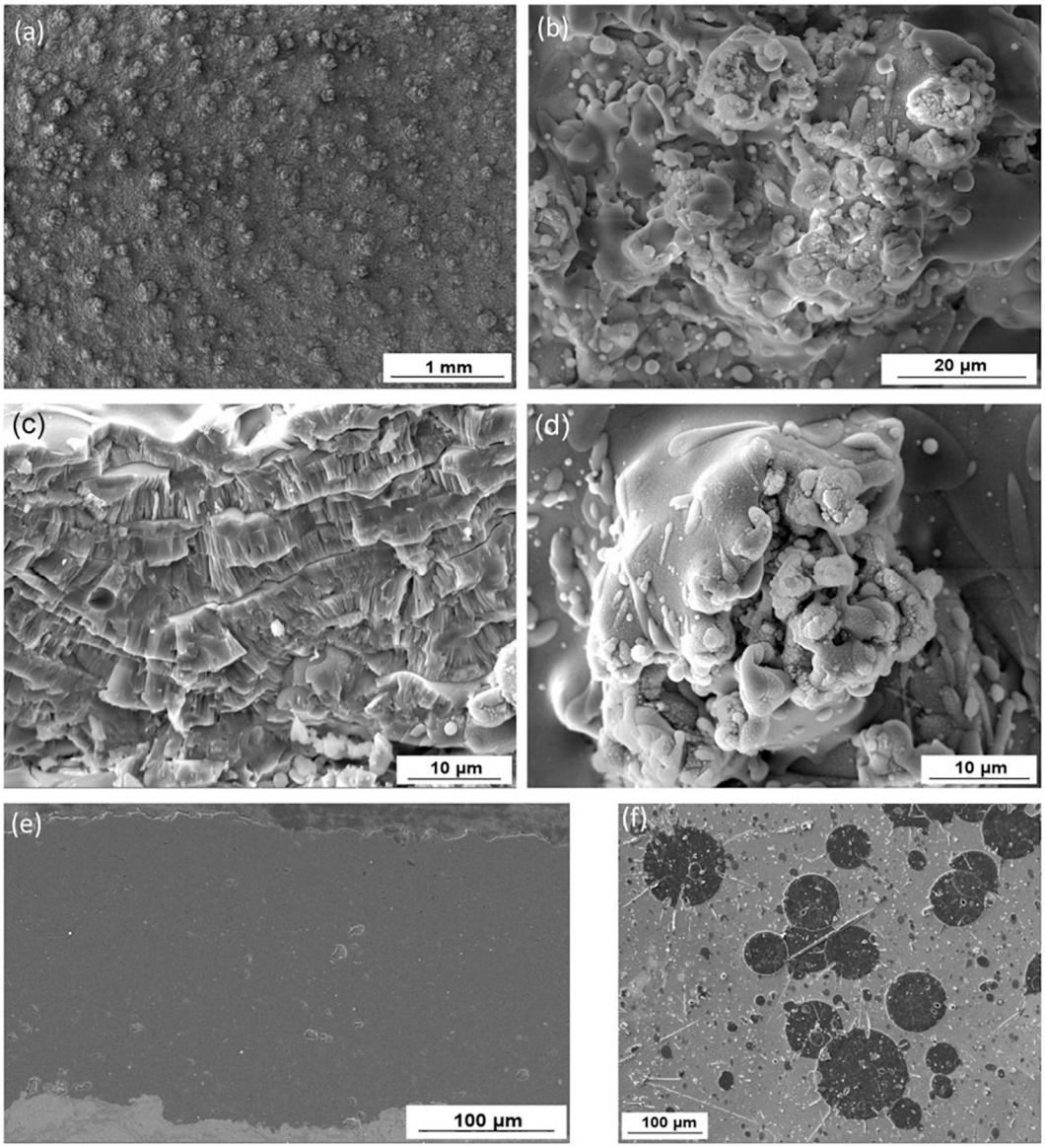

Fig. 8. Top surfaces (a, b, d), fracture surface (c), polished cross-section (e) and single scanning splats (f) of alumina coatings (SD = 350 mm, Sample D).

Table 2
Experimental parameters of coatings.

Sample	A	B	C	D
Spraying distance/mm	200	250	300	350
Current/A	160	160	160	160
Voltage/V	157.5	158	158	157.7

super-long spraying distances from 200 mm to 350 mm. Fig. 9 demonstrates the microscopic schematic diagram of the coating deposition process. The maximum diameter of single splats is < 100 μm. The overlapped splats form the layers of coatings (Fig. 9b), which include voids or pores at the cross-section (Fig. 9d). The multi – island protrusions at the top surface of coatings are formed with plenty of splats and their splashing duo to a very focused deposition spot when the plasma jet was impinging on the substrate. Finally, a very focused deposition spot, well-melted alumina particles and high reproducibility in several repeated scans of the plasma spray process are all contributed to the microstructure formation. The microstructure frameworks contain multi-island protrusions at the top surface, layers of typical lamellar structure at the fracture surface and polished cross section with voids or pores.

4. Discussions of coating physical performances

4.1. XRD results of the alumina coatings and powders

Fig. 10 showed the XRD results of four alumina coatings and the alumina powders. The initial alumina powder consisted of the α-

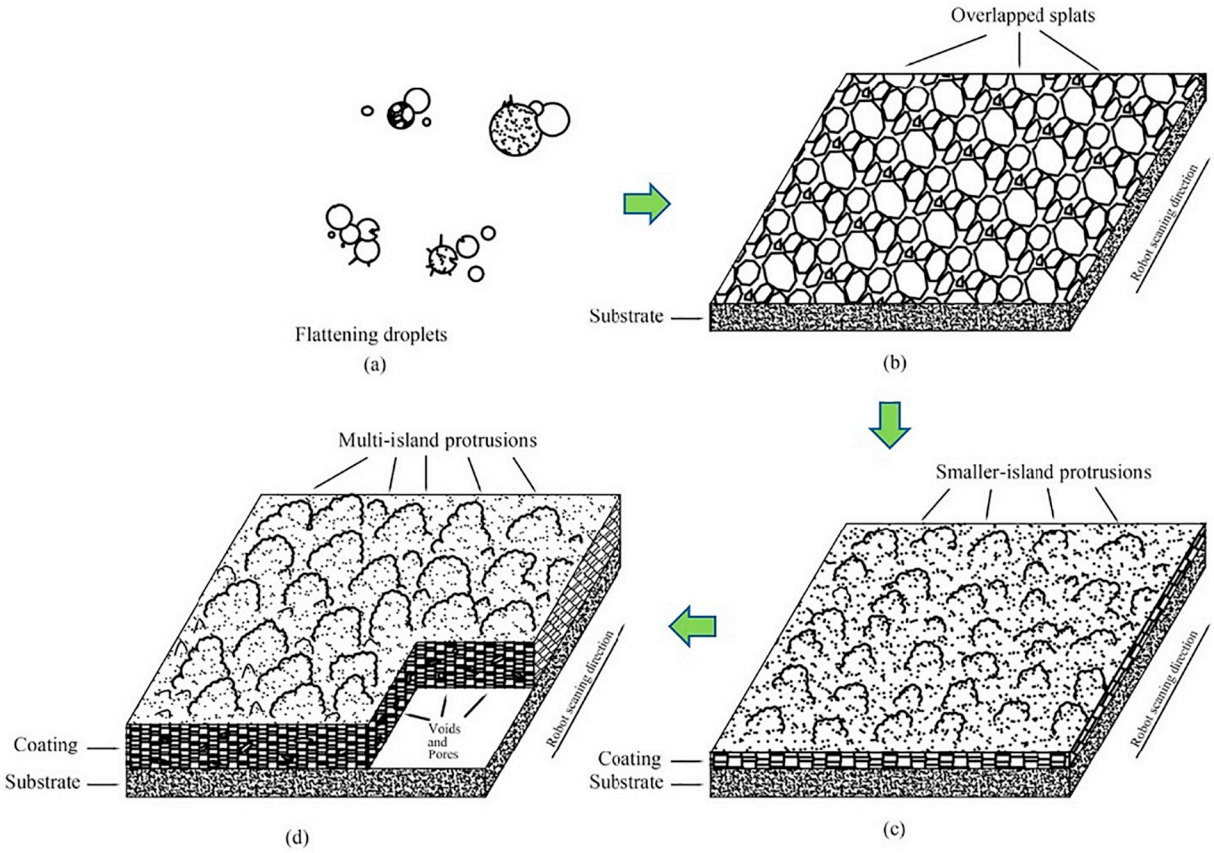

Fig. 9. Schematic diagram of the deposition process of alumina coatings, the initial deposited splats of (a); overlapped splats after several repeat times of robot-scanning (b); the formation of island-protrusions (c); the final microstructure diagram of coating (d).

phase. However, the γ-phase was the main phase in coatings that generated from the rapid solidification droplets during the atmospheric plasma spray process, which was consistent with other published results [18,19]. That means the powders were well-melted during spray process.

4.2. Porosity and hardness of alumina coatings

The apparent porosity and hardness at the cross section of four samples as functions of spraying distances were shown in Fig. 11. The distributions of porosity did not be changed in a widely range from the super long distance from 200 mm to 350 mm. The distributions of the hardness of coatings were at the mean value ranging from 11.1 to 12.8 GPa. Curran & Clyne, Bolelli et al. and Meng et al. also obtained the same results by using conventional atmospheric plasma spray methods [20–22].

4.3. Top surface roughness of alumina coatings

The top surface roughness (Ra) of four samples was demonstrated in Fig. 12 by the 3D Laser Scanning Microscope Methods (VK-9700, Violet Laser, Japan). The surface roughness of the alumina coatings in this study were all > 15 μm, which was also larger than that of other conventional plasma sprayed alumina coatings by Curran & Clyne [20]. Moreover, the sizes of top protrusion were also larger than the sizes of initial powders. That means the top protrusions of coatings were constituted of numerous overlapped alumina splats and without unmelted particles combined with the results of high-magnification SEM and the XRD results. The polygonal alumina particles were fully melted at different spraying distances in experiment.

4.4. Thermal conductivity of alumina coatings

The thermal diffusivity and thermal conductivity of four coatings at the temperature range from 273 K to 1273 K by the laser flash technique were shown in Figs. 13 and 14, respectively. Sampath et al. and Hao et al. that used the conventional APS method also obtained the same results [23,24]. The lamellar structure of the coatings constituted with voids and pores can enhance the phonon scattering and reduce the phonon mean free path in experiment. The microstructures and porosities distribution were recognized as vital factors in reducing the thermal conductivity between the four samples.

5. Conclusions

The alumina coatings were deposited by a newly laminar plasma spraying method in this paper. The refractory alumina particles can be fully melted during spray process in an atmospheric environment at

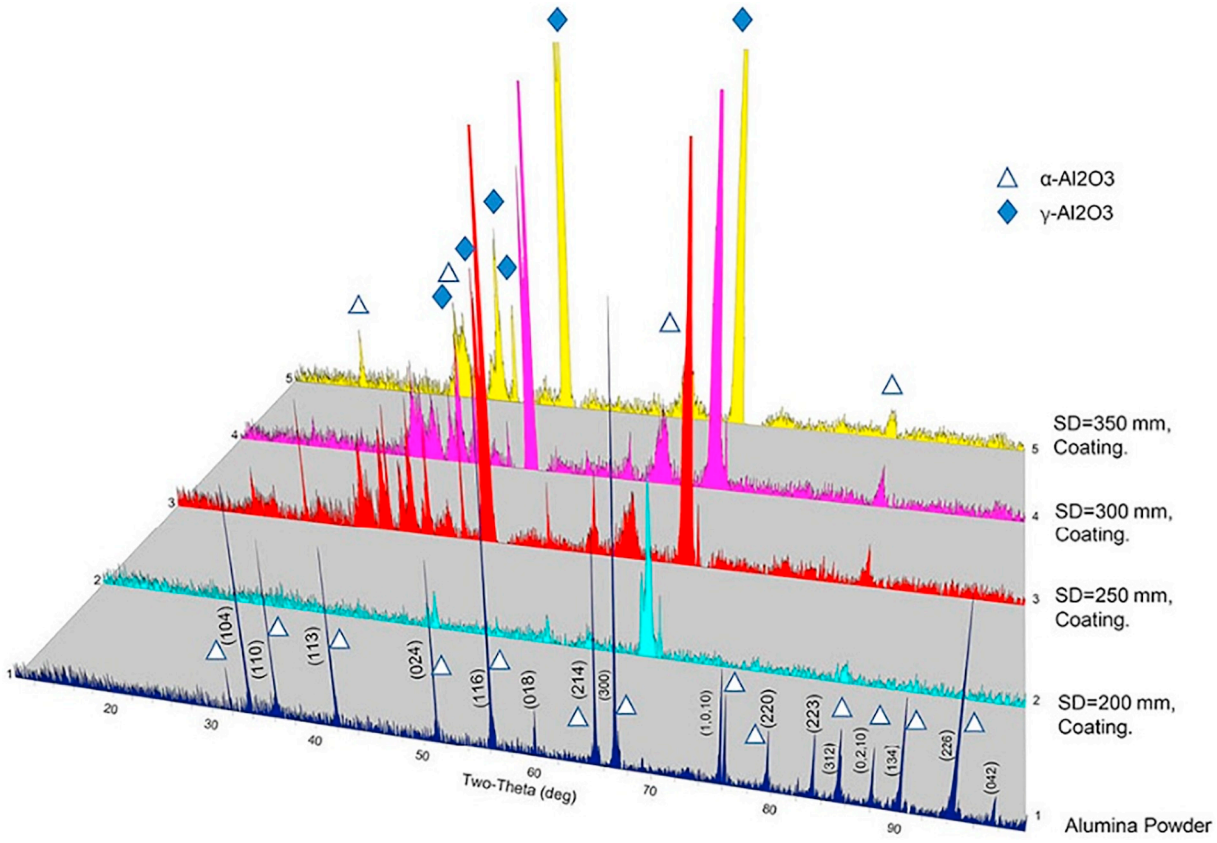

Fig. 10. XRD results of the four alumina coatings and the powders.

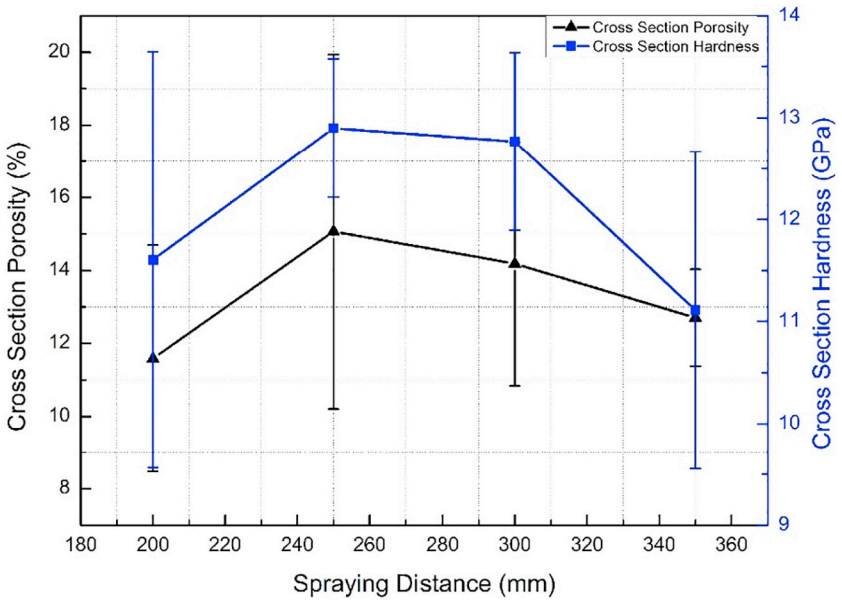

Fig. 11. Polished cross-section porosity and harness of the four alumina coatings.

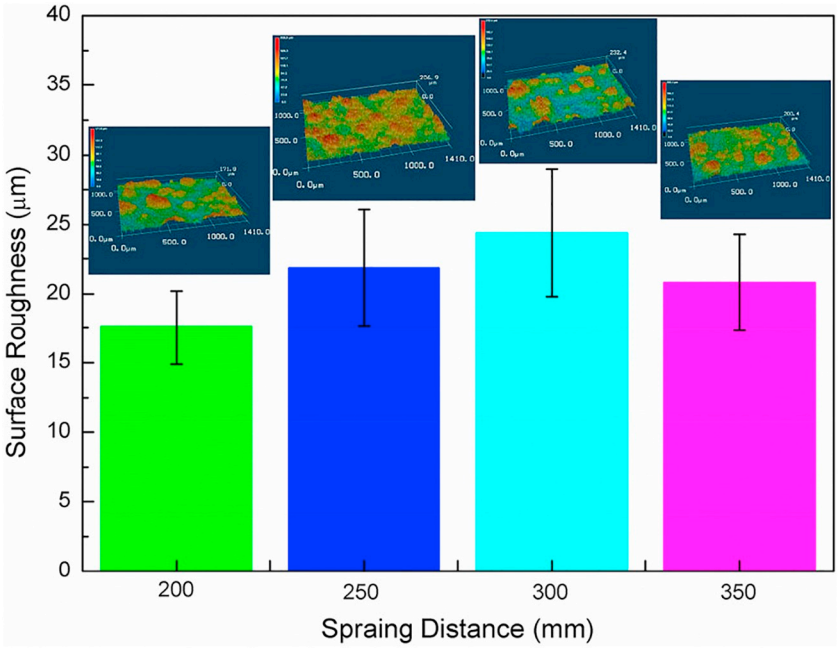

Fig. 12. Top surface roughness (Ra) of the four alumina coatings.

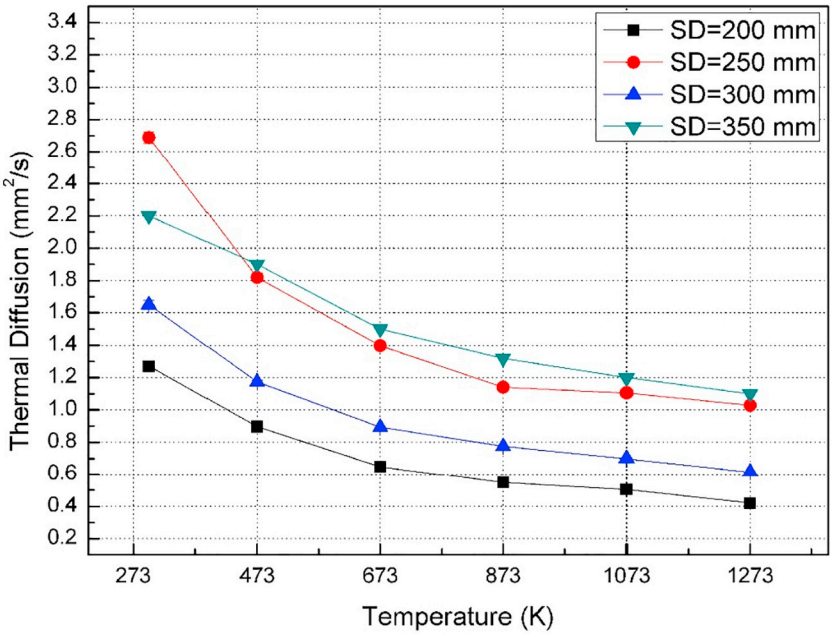

Fig. 13. Thermal diffusivity of the four alumina coatings.

four different spraying distances from 200 to 350 mm, although the working conditions were only at total gas flow rate of 14 slpm, output power of 25–26 kW and under more less working noise. The powders flight through a super-long heating and accelerating distance due to the distributions of lower particle velocity and higher particle surface temperature that compared with other current conventional atmospheric plasma spraying methods. A very focused deposition spot, well-melted alumina particles and high reproducibility in several repeated scans of spray process are all contributed to the microstructure formation. The microstructure frameworks contain multi-island protrusions at the top surface, layers of typical lamellar structure at the fracture surface and polished cross section with voids or pores. This atmospheric laminar plasma spraying method provides a new option for the thermal plasma technology and significantly improved the working environment for users.

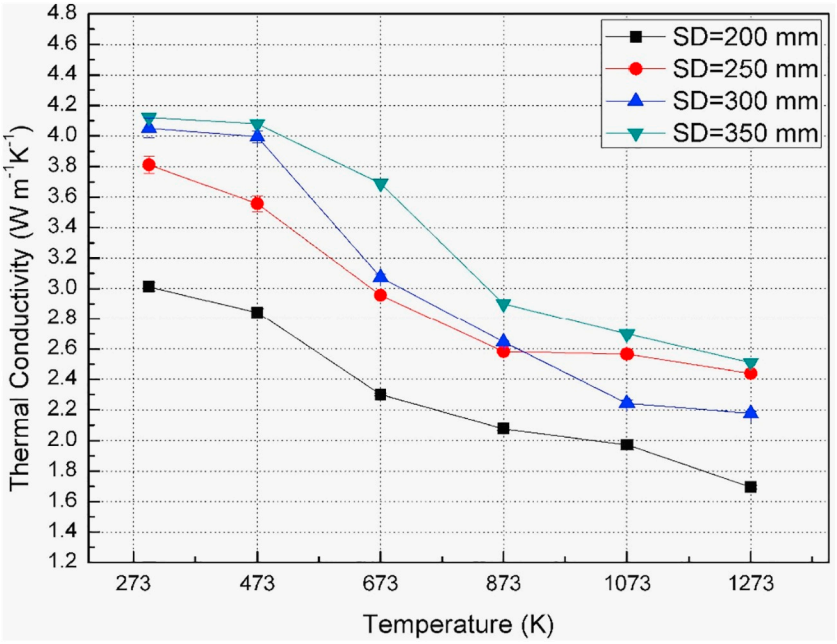

Fig. 14. Thermal conductivity of the four alumina coatings.

Acknowledgements

The authors are grateful to Mr. Jing-Xi Wang from Department of Materials Science and Engineering in Xi'an Jiaotong university for the help in preparation of specimens. This work was supported by the Natural Key R&D Program of China (Basic Research Project, Grant No. 2017YFB0306104) and National Natural Science Foundation of China (Grant No. 91860114), the PhD Short-term Academic Visiting Program of Graduate School of Xi'an Jiaotong University and National PhD Degree Program of the China Scholarship Council.

References

[1] Z. Duan, J. Heberlein, Arc instabilities in a plasma spray torch, J. Therm. Spray Technol. 11 (March) (2002) 44–51.
[2] E. Nogues, M. Vardelle, P. Fauchais, P. Granger, Arc voltage fluctuations: comparison between two plasma torch types, Surf. Coat. Technol. 202 (18) (2008) 4387–4393, https://doi.org/10.1016/j.surfcoat.2008.04.014.
[3] V. Rat, F. Mavier, J.F. Coudert, Electric arc fluctuations in DC plasma spray torch, Plasma Chem. Plasma Process. 37 (2017), https://doi.org/10.1007/s11090-017-9797-7.
[4] E. Pfender, Plasma jet behavior and modeling associated with the plasma spray process, Thin Solid Films 238 (1994) p228–p241.
[5] M.P. Planche, R. Bolot, C. Coddet, In-flight characteristics of plasma sprayed alumina particles: measurements, modeling, and comparison, J. Therm. Spray Technol. 12 (March) (2003) 101–111.
[6] C.J. Li, B. Sun, Microstructure and property of Al_2O_3 coating microplasma-sprayed using a novel hollow cathode torch, Mater. Lett. 58 (1–2) (2004) 179–183, https://doi.org/10.1016/S0167-577X(03)00441-5.
[7] Lidong Zhao, Klaus Seemann, Arne Fischer, E. Lugscheider, Study on atmospheric plasma spraying of Al_2O_3 using on-line particle monitoring, Surf. Coat. Technol. 168 (2003) 186–190, https://doi.org/10.14158/j.cnki.1001-3814.2010.20.028.
[8] S.H. Liu, C.X. Li, et al., A novel structure of YSZ coatings by atmospheric laminar plasma spraying technology, Scr. Mater. 153 (2018) 73–76.
[9] S.H. Liu, S.L. Zhang, C.X. Li, L. Li, J.H. Huang, J.P. Trelles, ... C.J. Li, Generation of Long Laminar Plasma Jets: Experimental and Numerical Analyses, Plasma Chem. Plasma Process. (2019) 1–18.
[10] S.H. Liu, C.X. Li, et al., Development of long laminar plasma jet on thermal spraying process: microstructures of zirconia coatings, Surf. Coat. Technol. 337 (2018) 241–249.
[11] Tecnar-Spray Process Individual Particle Characterization, http://www.tecnar.com/dpv-evolution/.
[12] 3D Laser Scanning Microscope User's Manual, https://www.keyence.com/ss/products/microscope/glossary/cat2/laser_scanning_confocal_microscopes/index.jsp.
[13] ASTM E1461, Standard Test Method for Thermal Diffusivity by the Flash Method, http://www.astm.org/DATABASE.CART/HISTORICAL/E1461-07.htm, (2007).
[14] S. Guessasma, G. Montavon, C. Coddet, Velocity and temperature distributions of alumina-titania in-flight particles in the atmospheric plasma spray process, Surf. Coat. Technol. 192 (1) (2005) 70–76, https://doi.org/10.1016/j.surfcoat.2004.03.020.
[15] Z. Yin, S. Tao, X. Zhou, C. Ding, Particle in-flight behavior and its influence on the microstructure and mechanical properties of plasma-sprayed Al2O3 coatings, J. Eur. Ceram. Soc. 28 (6) (2008) 1143–1148, https://doi.org/10.1016/j.jeurceramsoc.2007.09.050.
[16] E. Turunen, T. Varis, S.P. Hannula, A. Vaidya, A. Kulkarni, J. Gutleber, ... H. Herman, On the role of particle state and deposition procedure on mechanical, tribological and dielectric response of high velocity oxy-fuel sprayed alumina coatings, Mater. Sci. Eng. A 415 (1–2) (2006) 1–11, https://doi.org/10.1016/j.msea.2005.08.226.
[17] ISO 16787, Intelligent Transport Systems—Assisted Parking System (APS)—Performance Requirements and Test Procedures, https://www.iso.org/standard/73768.html, (2017).
[18] Xiaoxiao, Cheng, Shubing, Xingzhi, Study on performance of Al_2O_3 - based ceramics coating prepared by plasma spraying, Surf. Coat. Technol. 168 (99–103) (2010) 8.
[19] G.J. Yang, C.X. Li, C.J. Li, Characterization of nonmelted particles and molten splats in plasma-sprayed Al_2O_3 coatings by a combination of scanning electron microscopy, X-ray diffraction analysis, and confocal Raman analysis, J. Therm. Spray Technol. 22 (2–3) (2013) 131–137.
[20] J.A. Curran, T.W. Clyne, Thermo-physical properties of plasma electrolytic oxide coatings on aluminium, Surf. Coat. Technol. 199 (2–3) (2005) 168–176, https://doi.org/10.1016/j.surfcoat.2004.09.037.
[21] G. Bolelli, J. Rauch, V. Cannillo, A. Killinger, L. Lusvarghi, R. Gadow, Microstructural and tribological investigation of high-velocity suspension flame sprayed (HVSFS) Al_2O_3 coatings, J. Therm. Spray Technol. 18 (1) (2009) 35.
[22] F. Meng, C. Liu, F. Zhang, Z. Tian, W. Huang, Densification and mechanical properties of fine-grained Al_2O_3–ZrO_2 composites consolidated by spark plasma sintering, J. Alloys Compd. 512 (1) (2012) 63–67, https://doi.org/10.1016/j.jallcom.2011.09.015.
[23] S. Sampath, X. Jiang, J. Matejicek, A. Leger, A. Vardelle, Substrate temperature effects on splat formation, microstructure development and properties of plasma sprayed coatings Part I: case study for partially stabilized zirconia, Mater. Sci. Eng. A 272 (1) (1999) 181–188, https://doi.org/10.1016/S0921-5093(99)00459-1.
[24] S. Hao, C.-J. Li, G.-J. Yang, Influence of deposition temperature on the microstructures and properties of plasma-sprayed Al2O3 coatings, J. Therm. Spray Technol. 20 (1–2) (2010) 160–169, https://doi.org/10.1007/s11666-010-9591-z.